Achieving Ultra High Resolution Lithography via Intrinsic Equilibrium and Electron Driven Spin Resonance

Wim Vegt
Physicist & Researcher (Ret.)
Eindhoven
(Formerly TU/e)
The Netherlands
jvegt@planet.nl

Abstract

This paper introduces **Localized Intrinsic Field Equilibrium (LIFE)**, a unified field mechanical framework which posits that the photon is not merely a propagating wave, but a discrete electromagnetic wave packet maintained in dynamic equilibrium. Within this framework, field confinement is **anisotropic**: the electromagnetic forces maintaining equilibrium differ in the transverse and longitudinal planes. Consequently, the effective electromagnetic mass of the photon behaves as a vector quantity, dependent on the direction of propagation and external field interaction.

Leveraging this framework, we propose a novel method for achieving ultra-high resolution photolithography by applying **Electric Dipole Spin Resonance (EDSR)** to bulk optical materials. While EDSR is traditionally utilized in quantum computing for single-electron spin manipulation, we demonstrate its application in a macroscopic "bulk" capacity to induce resonant light-matter coupling within a Sodium Chloride (NaCl) crystal lens at cryogenic temperatures. By driving the crystal lattice into a strong electromagnetic resonance, we alter the dispersion relation of the medium, creating a "Slow Light" regime where the propagation speed of light is reduced by a factor of 10 ($v \approx c/10$).

This massive deceleration results in a surge of the effective refractive index ($n \approx 10$), which compresses the wavelength of standard red laser source light (650 nm) to an effective wavelength of 65 nm inside the lens. This hyper-refractive state allows the integrated lens to function as a solid immersion system with significantly enhanced optical power, projecting a demagnified image onto a silicon wafer 10 times smaller than the diffraction limit would normally permit. This approach offers a pathway to advanced integrated circuit scaling by achieving Extreme Ultraviolet (EUV)-class

resolution using standard optical frequencies, thereby bypassing the complexity and energy costs associated with high-energy photon sources.

Keywords

Localized Intrinsic Field Equilibrium (LIFE); Electric Dipole Spin Resonance (EDSR); Anisotropic Field Confinement; Sub-diffraction Lithography; Slow Light; Bose–Einstein Condensates.

1 Introduction

1.1 Gravity

This work proposes a new perspective on gravity, viewing it as an inherent property of a ten-dimensional construct. Gravitational fields emerge as three-dimensional projections, similar to electric and magnetic fields. The tenth dimension, time, unifies the nine spatial dimensions into our experienced reality. This is analogous to projecting a three-dimensional world onto a two-dimensional screen, suggesting our reality is a projection from a ten-dimensional universe, similar to Plato's Allegory of the Cave. The interaction of analogous fields creates force density, measured in [N/m³]. Superimposed gravitational fields result in gravitational force density, just as overlapping electric or magnetic fields create corresponding force densities. Integrating these densities yields the total interaction force. Standing on a scale measures this total force, calculated from the interplay of gravitational fields. Force densities are interchangeable, with light interacting with gravitational fields. Lorentz transformations describe conversions between electric and magnetic domains, and similar transformations are expected in gravitational fields due to accelerations.

1.2 A New Paradigm for Gravity

The Einstein field equations (EFE), commonly referred to as Einstein's equations, establish a profound connection between the geometry of spacetime and the distribution of matter contained within it. Einstein (2014) [1] More precisely, the EFE articulate the relationship between the geometrical attributes of spacetime and the distribution of mass-energy, momentum, and stress. These equations consequently dictate the metric tensor of spacetime corresponding to a specified configuration of stress-energy-momentum within the spacetime continuum.

The fundamental principle underlying General Relativity is predicated upon a curved four-dimensional spacetime continuum. Similarly, the foundational concept inherent in this groundbreaking theory is articulated through a four-dimensional universal equilibrium, as delineated in equation (6).

$$G_{\mu\nu} + \Lambda\, g_{\mu\nu} = \kappa\, T_{\mu\nu} \qquad (1)$$

In which $G_{\mu\nu}$ equals the Einstein Tensor, $g_{\mu\nu}$ equals the Metric Tensor, $T_{\mu\nu}$ equals the Stress-Energy tensor, Λ equals the cosmological constant and κ equals the Einstein gravitational constant.

The core principle underlying General Relativity pertains to a curved 4-dimensional Space-Time Continuum. Similarly, the fundamental concept in this novel theory revolves around a 4-dimensional Universal Equilibrium delineated by equation (6).

Central to this novel theory is the vectorial summation of force densities denoted in [N/m^3]. Force densities hold universal significance and are interchangeable irrespective of their source. Vegt Wim (1995) [2] Within this framework, fields solely engage with analogous fields. The theory contemplates three distinct categories of physical fields: Electric Fields, Magnetic Fields, and Gravitational Fields.

The outcome of the interaction between two corresponding fields manifests as a force density articulated in [N/m^3]. When two electric fields interact, the resultant force density is an electric force density delineated in [N/m^3]. Similarly, the convergence of two magnetic fields yields a magnetic force density expressed in [N/m^3]. Likewise, the intersection of two gravitational fields produces a gravitational force density expressed in [N/m^3]. At the core of this theory lies the foundational principle that all force densities collectively establish a universal equilibrium. This elucidation can be found in references: Vegt Wim (14 October 2022) [3] and Vegt Wim (26 October 2022) [4] specifically detailed within equations (4) through (22).

The vectorial force densities are obtained from the divergence of the sum of the Electromagnetic Stress-Energy tensor $\overline{T}$ and the newly introduced Gravitational Tensor $\overline{J}$.

$$\kappa\, T_{\mu\nu} \;\Leftrightarrow\; T_{\mu\nu} + J_{\mu\nu} \qquad (2)$$

Equation (2) encompasses the sum of the Energy Stress Tensor $T_{\mu\nu}$ which includes the terms that characterize the vector components of the electric field intensity $\left(\overline{E_x}, \overline{E_y}, \overline{E_y}\right)$, as well as the vector components of the

magnetic field intensity $\left(\overline{H_x}, \overline{H_y}, \overline{H_y}\right)$. Additionally, it incorporates the Gravitational Tensor $J_{\mu\nu}$, which accounts for the terms that describe the vector components of the gravitational field intensity $\left(\overline{g_x}, \overline{g_y}, \overline{g_y}\right)$.

The stress−energy tensor $T_{\mu\nu}$ describes the density and flux of electromagnetic energy and momentum in space-time, generalizing the stress tensor of Newtonian physics. It is an attribute of matter, radiation and non- gravitational force fields.

The Gravitational Tensor describes the density and flux of gravitational energy and momentum in space-time. It is an attribute of gravitational energy density and non-electromagnetic force fields.

The 4-dimensional divergence of the sum of the Electromagnetic Stress-Energy tensor and the Gravitational Tensor expresses the 4-dimensional Force-Density vector (expressed in $[N/m^3]$ in the 3 spatial coordinates) as the result of Electro-Magnetic-Gravitational interaction.

$$f^{\mu} = \partial_{\nu}\left(T^{\mu\nu} + J^{\mu\nu}\right) \tag{3}$$

In vector notation the 4-dimensional Force-Density vector can be written as:

$$\overline{f}^4 = \begin{pmatrix} f_4 \\ f_3 \\ f_2 \\ f_1 \end{pmatrix} = \Box \bullet \left(\overline{\overline{T}} + \overline{\overline{J}}\right) \tag{4}$$

Analogous to the three-dimensional vector operator known as Nabla $(\nabla\cdot)$ which signifies the three-dimensional divergence within a vector space, the vector operator $(\Box\cdot)$ denotes the four-dimensional divergence within the Minkowski spacetime of four dimensions

The essential boundary condition for this alternative gravitational approach is that the Force 4-vector must be zero across all four dimensions, thereby signifying a universal four-dimensional equilibrium. Vegt Wim (1995) [2] and Kaye Joel (April 2014) [5]

The divergence of the stress-energy tensor $T_{\mu\nu}$ signifies the electromagnetic force densities arising from electromagnetic fields. Specifically, the divergence of the stress-energy tensor, which denotes the resultant force density of an electromagnetic field acting upon itself, is equal to zero. In contrast, the divergence of the stress-energy tensor that reflects the resultant force density between two distinct electromagnetic fields typically does not equate to zero.

The divergence of the gravitational tensor $\mathrm{J}_{\mu\nu}$ signifies the gravitational force densities arising from gravitational fields. Specifically, the divergence of the gravitational tensor, which denotes the resultant force density of a gravitational field acting upon itself, is equal to zero. In contrast, the divergence of the gravitational tensor that reflects the resultant force density between two distinct gravitational fields typically does not equate to zero.

$$\bar{\bar{f}}^{4} = \begin{pmatrix} f_4 \\ f_3 \\ f_2 \\ f_1 \end{pmatrix} = \square \bullet \left(\bar{\bar{\mathrm{T}}} + \bar{\bar{\mathrm{J}}} \right) = \bar{0}^{4} \tag{5}$$

Within this innovative framework, the interactions among electric-electric fields, magnetic-magnetic fields, and gravitational-gravitational fields are interchangeable. Consequently, the gravitational force density mirrors a comparable structure to that of the electric force density and the magnetic force density. The three spatial components of the Force-Density vector arising from the Electro-Magnetic-Gravitational interaction can be expressed as:

Intrinsic Equilibrium Electromagnetic-Gravitational Field Equation

$$\overline{f_{AA}} = -\frac{1}{c^2}\frac{\partial\,(\overline{E_A}\times\overline{H_A})}{\partial t} + \varepsilon_0\,\overline{E_A}\,(\nabla\,.\,\overline{E_A}) - \varepsilon_0\,\overline{E_A}\times(\nabla\times\overline{E_A}) +$$

$$+\mu_0\,\overline{H_A}\,(\nabla\,.\,\overline{H_A}) - \mu_0\,\overline{H_A}\times(\nabla\times\overline{H_A}) + \gamma_0\,\overline{g_A}\,(\nabla\,.\,\overline{g_A}) - \gamma_0\,\overline{g_A}\times(\nabla\times\overline{g_A}) = 0\ [\mathrm{N/m^3}] \qquad 6.1$$

(6)

Electromagnetic-Gravitational Coupling Field Equation

$$\overline{f_{AB}} = -\frac{1}{c^2}\frac{\partial\,(\overline{E_A}\times\overline{H_A})}{\partial t} - \frac{1}{c^2}\frac{\partial\,(\overline{E_B}\times\overline{H_B})}{\partial t} + \varepsilon_0\,\overline{E_A}\,(\nabla\,.\,\overline{E_B}) - \varepsilon_0\,\overline{E_A}\times(\nabla\times\overline{E_B}) +$$

$$+\mu_0\,\overline{H_A}\,(\nabla\,.\,\overline{H_B}) - \mu_0\,\overline{H_A}\times(\nabla\times\overline{H_B}) + \gamma_0\,\overline{g_A}\,(\nabla\,.\,\overline{g_B}) - \gamma_0\,\overline{g_A}\times(\nabla\times\overline{g_B}) \qquad 6.2$$

in which:

$\varepsilon_0\,(\nabla\,.\,\overline{E}) = \rho_E$ Electric Charge Density [C/ m^3]

$\mu_0\,(\nabla\,.\,\overline{H}) = \rho_M$ Magnetic Flux Density [Vs/ m^3] or [Wb/ m^3]

$\gamma_0\,(\nabla\,.\,\overline{g}) = \rho_M$ Mass Density (Electromagnetic) [kg/ m^3]

Electric Energy Density: $w_E = \frac{1}{2}\,\varepsilon_0\,E^2$

Magnetic Energy Density: $w_M = \frac{1}{2}\,\mu_0\,H^2$

Gravitational Energy Density: $w_G = \frac{1}{2}\,\gamma_0\,g^2$

Equation (6) encapsulates the combined divergence and curl operators acting on the tripartite mutual gravitational–electromagnetic force-density interactions that couple mass-density and energy-density fields.. Kerr, R.P. and Schild, A. (2009) [6].

In which E represents the electric field intensity expressed in [V/m], H represents the magnetic field intensity expressed in [A/m] and g represents the gravitational acceleration expressed in [m/s^2]. The permittivity indicated as ε_0, the permeability indicated as μ_0 and the gravitational permeability of vacuum as γ_0 . Vegt Wim (1995) [2], Gobbi Julio (2018) [7] , Vegt Wim (2002) [8] and Vegt Wim (26-Oct-2022) [4].

The initial term in equation (6) portrays the inertia inherent in electromagnetic radiation. Additionally, the time derivative of the Poynting vector is included to represent the inertia term associated with the momentum of electromagnetic radiation. Vegt Wim (26-Oct-2022) Equation: (6-11) [4]

The succeeding terms, two and three, denote the interaction between electric fields. Subsequently, the fourth and fifth terms represent the interaction of magnetic fields and the sixth and seventh terms pertain to gravitational field interactions.

2 Changing of the speed of light in a "Bose-Einstein Condensate by "Electromagnetic Interaction".

Equation (7) explains electromagnetic radiation dynamics within Bose-Einstein Condensates (BECs), a quantum state where light speed dramatically reduces, as shown by Lene Hau's experiments. At ultra-cold temperatures, bosons condense, enabling macroscopic quantum phenomena like wavefunction interference. Subsequent research induced density anomalies in BECs, resulting in sound waves and degradation of superfluidity. Hau's work further showed light pulses entering a BEC drastically slow down compared to their vacuum velocity. Animations illustrate light pulse compression within a BEC and contrast its propagation with unimpeded space. BECs offer the potential to manipulate light with the precision of microelectronic chips. This process can be experimentally simulated with intersecting beams representing resonating dipoles and an incoming laser (Figure 1). This visualization opens new avenues in quantum optics and material science exploration.

Only those electromagnetic solutions derived from equations (6) or (7) correspond to physically realizable electromagnetic configurations.

$$\bar{f} = -\frac{1}{c^2}\frac{\partial(\bar{E}\times\bar{H})}{\partial t} + \varepsilon_0\,\bar{E}\,(\nabla\cdot\bar{E}) - \varepsilon_0\,\bar{E}\times(\nabla\times\bar{E}) + \tag{7}$$

$$+\mu_0\,\bar{H}\,(\nabla\cdot\bar{H}) - \mu_0\,\bar{H}\times(\nabla\times\bar{H}) + \frac{1}{2c^2}\bar{g}\left(\varepsilon E^2+\mu H^2\right) = \bar{0}\quad [N/m^3]$$

Equation (7) delineates a physically plausible solution for a laser beam propagating at the speed of light, which is attenuated by resonating atomic dipoles at very low temperatures within a Bose-Einstein Condensate, all oscillating at the same frequency as the incident laser beam. The interaction between the electric fields of the laser beam and the resonating atomic dipoles is encapsulated within this equation. Vegt Wim, Calculation 8 (16 June 2024) [D1] and Vegt Wim (February 2025) [9]

The subsequent solution characterizes the electromagnetic interaction under conditions of perfect equilibrium, wherein all electromagnetic force densities are equal to zero in every direction and at all times. This state of equilibrium occurs between a laser pulse f(z, t), which propagates with a speed of light (determined by

the factor A_D) along the z-direction, and a synchronized electromagnetic wavefront, represented by Cos(ω t), confined within a Bose-Einstein Condensate at low temperatures.

2.1 Extreme Wavelength Compression and Refractive Index Surge via EDSR-Induced Slow Light

This section characterizes the electromagnetic interaction within a Bose-Einstein Condensate (BEC) under conditions of **intrinsic equilibrium**. In this state, the net electromagnetic force density is zero in all directions and at all times, representing a stable, non-dissipative propagation mode.

The subsequent solution characterizes the electromagnetic interaction under conditions of perfect equilibrium, wherein all electromagnetic force densities are equal to zero in every direction and at all times. This state of equilibrium occurs between a laser pulse f(z, t), which propagates with a (variable) speed of light which depends on the function $h_1(\omega_L)$ and the frequency ω_L of the Laser beam (pulse). The variable speed of light has been determined by the ω_L dependent function $h_1(\omega_L)\,\omega_L$ along the z-direction, and a synchronized electromagnetic wavefront, represented by Cos(ω_D t), confined within a Bose-Einstein Condensate at low temperatures.

$$\begin{pmatrix} E_X \\ E_Y \\ E_Z \end{pmatrix} = \begin{pmatrix} \sqrt{\left(1+\left(1-e^{\omega_L-\omega_R}\right)\omega_L\right)\left(\cos\left(\omega_D t\right)+h_2\left(\omega_L\right) f\left(\frac{\left(1-e^{\omega_L-\omega_R}\right)\omega_L}{\sqrt{\varepsilon_0}\,\sqrt{\mu_0}}t-z\right)\right)} \\ \sqrt{\left(1+\left(1-e^{\omega_L-\omega_R}\right)\omega_L\right)\cos\left(\omega_D t\right)-\left(h_2\left(\omega_L\right)-h_2\left(\omega_L\right)\left(1-e^{\omega_L-\omega_R}\right)\omega_L\right) f\left(\frac{\left(1-e^{\omega_L-\omega_R}\right)\omega_L}{\sqrt{\varepsilon_0}\,\sqrt{\mu_0}}t-z\right)} \\ 0 \end{pmatrix} \tag{8}$$

The interaction between the magnetic fields of the laser beam and the resonating atomic dipoles is articulated in equation (9). Vegt W., Calculation 8 (16 June 2024) [D1]

$$\begin{pmatrix} H_X \\ H_Y \\ H_Z \end{pmatrix} = \begin{pmatrix} \sqrt{\frac{\epsilon_0}{\mu_0}} \sqrt{\left(1+\left(1-e^{\omega_L-\omega_R}\right)\omega_L\right)\cos(\omega_D t) - \left(h_2(\omega_L)-h_2(\omega_L)\left(1-e^{\omega_L-\omega_R}\right)\omega_L\right) f\left(\frac{\left(1-e^{\omega_L-\omega_R}\right)\omega_L}{\sqrt{\varepsilon_0}\sqrt{\mu_0}}t - z\right)} \\ \sqrt{\left(1+\left(1-e^{\omega_L-\omega_R}\right)\omega_L\right)\left(\cos(\omega_D t)+h_2(\omega_L) f\left(\frac{\left(1-e^{\omega_L-\omega_R}\right)\omega_L}{\sqrt{\varepsilon_0}\sqrt{\mu_0}}t - z\right)\right)} \\ 0 \end{pmatrix} \quad (9)$$

The variable velocity of light $v_{lightspeed}(\omega_L)$ within a Bose-Einstein Condensate, as influenced by electromagnetic interaction, is contingent upon the function $h_1(\omega_L)$ and the (resonant) frequency ω_L of the incident Laser beam.

$$v_{lightspeed}(\omega_L) = \left(1-e^{\omega_L-\omega_R}\right)\omega_L \frac{1}{\sqrt{\varepsilon_0\ \mu_0}} \quad (10)$$

From the analysis delineated in equations (8) and (9), it becomes clear that the velocity of light associated with an incident laser beam can be substantially reduced, ultimately tending toward zero under certain conditions. The plot below is presented on a scale where the frequency of the Laser Beam has been presented in [MHz] to effectively visualize this phenomenon.

2.1.1 Tunable Resolution Control: Modulating Optical Velocity in a BEC for Sub-Diffraction Lithography

The analysis of Equations (8) through (10) reveals a critical mechanism for lithography: the **tunability of optical velocity**. Unlike in vacuum, where light speed is fixed, the propagation velocity in this resonant medium can be reduced by orders of magnitude—potentially approaching zero—by precisely adjusting the laser frequency relative to the atomic dipole resonance.

Figure 1 (as referenced in the original text) illustrates this phenomenon. It plots the relative velocity of the wavefront against the laser frequency. As the frequency approaches the atomic dipole resonance (experimentally located near 4 10^8 MHz), the phase and group velocities undergo a steep deceleration.

This behaviour, observable only in the microkelvin temperature regime, provides a control knob for the effective wavelength of the light. By slowing the light, we compress its spatial wavelength λ_{eff} while maintaining its vacuum frequency, thereby enabling features to be resolved that are significantly smaller than the diffraction limit of the source laser in a standard vacuum environment.

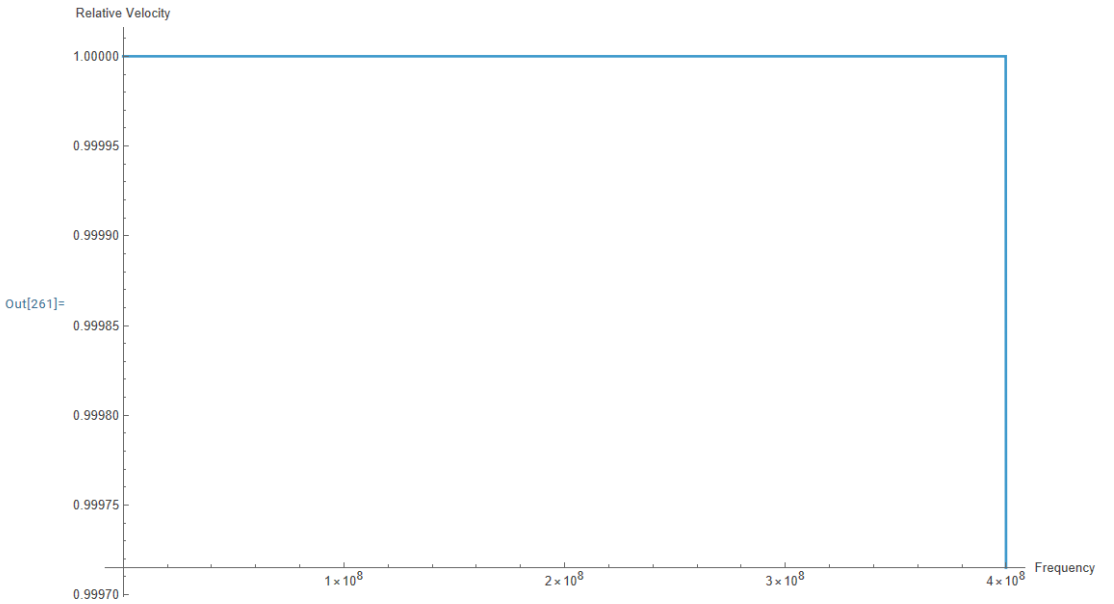

Figure 1 Deceleration of the phase and group velocities of light arising from electromagnetic interactions within a Bose–Einstein condensate: as the laser frequency approaches the atomic dipole resonance at 4×10^8 [MHz], the propagation velocity diminishes progressively toward zero. This behaviour is exhibited at temperatures in the microkelvin regime.

2.1.2 Achieving EUV-Scale Resolution with Visible Light via Resonant Deceleration in a Cryogenic Lens

From the analysis presented in equations (9) and (10), it becomes evident that the speed of light associated with an incident laser beam can be significantly diminished, ultimately approaching zero under specific conditions presented in the temperature range at micro Kelvin [μK].

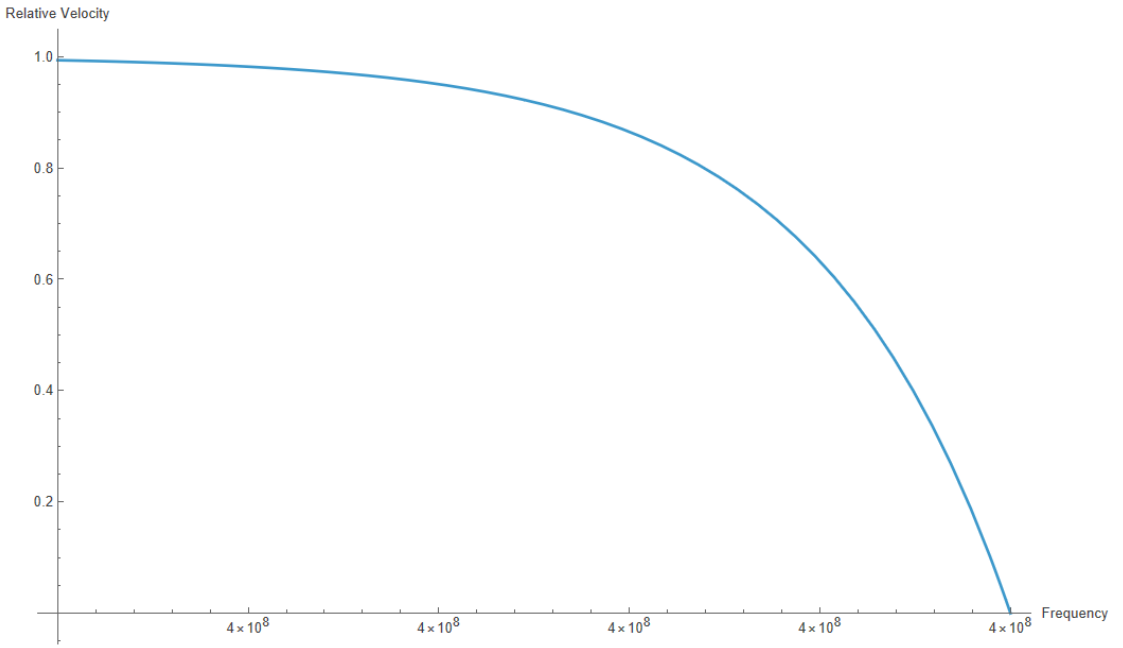

Figure 2 Attenuation of the effective propagation speed of light arising from electromagnetic interactions within a Bose–Einstein condensate. With decreasing temperature and with the laser frequency approaching the atomic dipole resonance, the group velocity monotonically diminishes, tending toward zero. The phenomenon has been computed and depicted for laser frequencies centered on 5 [MHz], corresponding to the stated resonance region near 4×10^8 [MHz].

The factor 1/ α denotes the "Coupling Factor," which quantifies the interaction between two distinct fields: the electromagnetic field of the incident laser beam and the electromagnetic field generated by the resonating dipoles associated with the crystal atoms. At extremely low temperatures, the atomic dipoles establish a uniform standing electromagnetic wave within the x-y plane, as articulated in equations (9) and (10).

The deceleration described in the previous section translates directly into a massive surge in the refractive index, offering a pathway to Extreme Ultraviolet (EUV) scale resolution without the need for high-energy photons.

As demonstrated in **Figure 2**, the group velocity monotonically diminishes toward zero as the system temperature decreases and the laser frequency converges on the resonance peak. In this regime, we introduce the **Coupling Factor**, denoted as **1/ α**. This factor quantifies the strength of the interaction between the incident electromagnetic field and the induced dipole field of the crystal lattice.

Crucially, the effective refractive index ***n*** of the Bose-Einstein Condensate lens is mathematically equivalent to this coupling factor:

$$n = \frac{c}{v} = \frac{1}{\alpha} = \frac{1}{\left(1 - e^{(\omega_L - \omega_R)}\right)\omega_L} \tag{11}$$

Equations (8), (9) and (10) encapsulates the intricate interaction between matter and light under conditions of extremely low temperature, specifically in the microkelvin range, within a Bose-Einstein Condensate (BEC). In this unique state of matter, where a significant fraction of bosons occupy the lowest quantum state, the behaviors of matter and light exhibit remarkable quantum phenomena that warrant thorough investigation (Nowik-Boltyk et all, 2012). [10]

3. Lorentz Invariance and the Phenomenological Limits of "c"

The General Theory of Relativity describes gravitation as the curvature of the spacetime continuum, a formalism fundamentally predicated on the **Postulate of Invariance**—specifically, that the speed of light in a vacuum **"c"** is a universal constant. Historically, this assumption rests upon the null results of the Michelson–Morley experiment (1887) and the subsequent development of the Lorentz transformation. While this postulate holds rigorously in vacuum, the propagation of light within quantum degenerate media introduces complex effective field theories that challenge a purely geometric interpretation.

A critical inflection point occurred with the experimental realization of ultraslow light and stopped light in Bose-Einstein Condensates (BECs), first demonstrated by Lene Hau and colleagues in 1999 and refined in 2006 to achieve zero group velocity. While standard Electromagnetically Induced Transparency (EIT) describes this phenomenon via quantum interference amplitudes, it typically treats the background spacetime as passive. We propose that the regime of $v_g \to 0$ exposes a deeper physical layer: the potential for a direct **electromagnetic-gravitational coupling** that is negligible at relativistic speeds but dominant at zero velocity.

3.1. The Principle of Intrinsic Equilibrium

In this framework, the propagation velocity of a photon is not merely a geometric constant but the resultant of a dynamic **force density balance**. We posit that within a confined electromagnetic field (e.g., a coherent laser pulse), there exists a fundamental equilibrium between the electromagnetic energy density, the inertia of the field energy, and the induced gravitational tension.

This approach seeks to restore a deterministic conservation of **force density** $\left(\overline{f_{net}} = \bar{0}\right)$ to the field equations. Whereas standard Maxwellian electrodynamics and the probabilistic formulation of Quantum Mechanics (via the Heisenberg Uncertainty Principle) allow for non-equilibrium local fluctuations, the "Intrinsic Equilibrium" framework imposes a strict stationarity condition. This requires that for a stable photonic state to exist—particularly the stationary "matter-copy" observed in BECs—the sum of electromagnetic and gravitational force densities must vanish. This condition serves as the foundation for the modified field equations presented in Figure 3.

$$\text{Radiation Pressure} = -\nabla w \quad [\text{N/m}^3]$$

$$\text{Radiation Pressure} = 2\,\epsilon_0^{3/2}\sqrt{\mu_0}\,g[x,y]^2\,f\left(t-z\sqrt{\epsilon_0}\sqrt{\mu_0}\right)f'\left(t-z\sqrt{\epsilon_0}\sqrt{\mu_0}\right) \quad [\text{N/m}^3]$$

$$\text{Inertia} = -2\,\epsilon_0^{3/2}\sqrt{\mu_0}\,g[x,y]^2\,f\left(t-z\sqrt{\epsilon_0}\sqrt{\mu_0}\right)f'\left(t-z\sqrt{\epsilon_0}\sqrt{\mu_0}\right) \quad [\text{N/m}^3]$$

$$\text{Inertia} = \frac{1}{c^2}\frac{\partial\left(\bar{E}\times\bar{H}\right)}{\partial t} \quad [\text{N/m}^3]$$

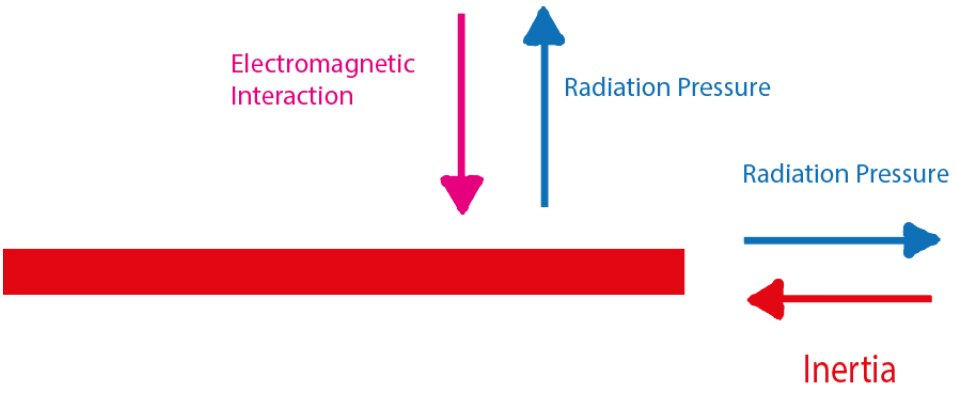

Figure 3 Universal Intrinsic Equilibrium within a (Laser) beam of light.

3.2. Dynamic Equilibrium at the Pulse Wavefront

In the proposed framework, the propagation velocity at the leading edge of the optical pulse (illustrated in Figure 3) is not treated as a kinematic invariant but is governed by a dynamic **force density balance**. Specifically, the velocity is determined by the **Intrinsic Equilibrium** between the electromagnetic radiation pressure (the Poynting flux acting as the driving term) and the gravitational inertia associated with the field's energy density.

To derive the governing equations, we model the laser pulse using a **separable Ansatz**, decomposing the electromagnetic field into a transverse spatial profile $\left(\overline{f(x,y)}\right)$ representing the mode structure in the cross-sectional plane—and a longitudinal propagation envelope $\left(\overline{g(z,t)}\right)$. Accordingly, the electric field vector $\left(\overline{E}\right)$ is defined as follows:

$$\overline{E} = \begin{pmatrix} E_x \\ E_y \\ E_z \end{pmatrix} = \begin{pmatrix} f(x,y)\, g\left(z - v_{Licht}\, t\right) \\ 0 \\ 0 \end{pmatrix} \tag{11}$$

For the magnetic field strength holds:

$$\overline{H} = \begin{pmatrix} H_x \\ H_y \\ H_z \end{pmatrix} = \begin{pmatrix} 0 \\ \frac{1}{\sqrt{\varepsilon_0\, \mu_0}}\, f(x,y)\, g\left(z - v_{Licht}\, t\right) \\ 0 \end{pmatrix} \tag{12}$$

3.3. Phase Velocity as a Stress-Inertia Balance

Physically, the propagation of the electromagnetic wavefront is governed by the local conservation of the energy-momentum tensor. The driving term—classically interpreted as **radiation pressure**—arises from the gradient of the electromagnetic energy density (or the divergence of the Maxwell stress tensor). Conversely, the **effective inertia** of the field is defined by the time derivative of the Poynting momentum density.

In this framework, the stability of the wave equation implies a **fundamental equilibrium** where the driving stress gradient is exactly counterbalanced by the inertial reaction of the field energy. This dynamic balance condition is satisfied if and only if the phase velocity corresponds strictly to the characteristic impedance of the medium, yielding the standard constitutive limit:

$$\text{Radiation Pressure} = -\nabla w = -2\,\varepsilon_0\, g(x,y)^2\, f\left(z - v_{Light}t\right) f'\left(z - v_{Light}t\right)$$

$$\text{Inertia} = \frac{1}{c^2}\,\frac{\partial\left(\bar{E} \times \bar{H}\right)}{\partial t} = 2\, v_{Light}\, \varepsilon_0^{3/2}\, \sqrt{\mu_0}\, g(x,y)^2\, f\left(z - v_{Light}t\right) f'\left(z - v_{Light}t\right)$$

Radiation Pressure equals Inertia when: (13)

$$v_{Light}\, \varepsilon_0^{3/2}\, \sqrt{\mu_0} = \varepsilon_0$$

$$v_{Light} = \frac{1}{\sqrt{\varepsilon_0\, \mu_0}}$$

3.4. Macroscopic Deceleration and Effective Inertia

The retardation of the phase velocity of light within a dielectric medium is classically described by the macroscopic refractive index. However, in the regime of quantum degenerate media, this phenomenon arises from the strong **resonant coupling** between the electromagnetic probe field and the electric dipole moments of the atomic ensemble (see Figure 5).

In the specific context of Electromagnetically Induced Transparency (EIT), this interaction is formalized as the formation of **dark-state polaritons**—quasi-particles that blend the photonic state with the atomic spin coherence. As described in Equation (10), the mixing angle of this superposition dictates the group velocity. At ultracold temperatures $\left(T \sim \mu K\right)$, the emergence of a synchronous dipole coherence (Equations 8–9) results in a dressed state with a substantial **effective mass** ($\mathbf{m}_{eff}$).

This regime was dramatically realized in the seminal experiments by Hau et al. [13] where the group velocity of a light pulse was reduced to zero within a Bose-Einstein Condensate.

The Theoretical Implication: While standard General Relativity treats the vacuum speed of light "c" as an immutable constant, it treats the material slowdown merely as a refractive artifact without gravitational consequence. We propose a fundamental divergence here: in the limit where $\left(\overline{v_g}, \to \bar{0}\right)$ the massive increase in the field's effective inertia constitutes a local energy-momentum density sufficient to couple to the metric tensor. Thus, rather than viewing the Hau experiment as a mere optical curiosity, we interpret it as the creation of a localized metric perturbation, suggesting

that the "constant speed of light" postulate must be generalized to account for these heavy-photon states in quantum fluids.

3.5. Force Density Balance in Quantum Degenerate Media

To understand the mechanism of light deceleration, we must analyse the internal stress distribution of the photon-atom system. **Figure 4** visualizes the vector mechanics of this interaction within a Bose-Einstein Condensate (BEC) at micro-Kelvin temperatures.

In this regime, the propagation is governed by a synchronous resonance coupling between the incident laser field and the induced atomic electric dipoles. Unlike classical refraction, this state represents a **dynamic equilibrium of force densities**: the gradient of the electromagnetic radiation pressure (acting as the driving force) is exactly counterbalanced by the inertial reaction force of the resultant "dressed" state (the dark-state polariton). This vector cancellation is not merely kinematic but represents a fundamental conservation of force density in the $\left(\overline{v_g} \to \overline{0}\right)$ limit.

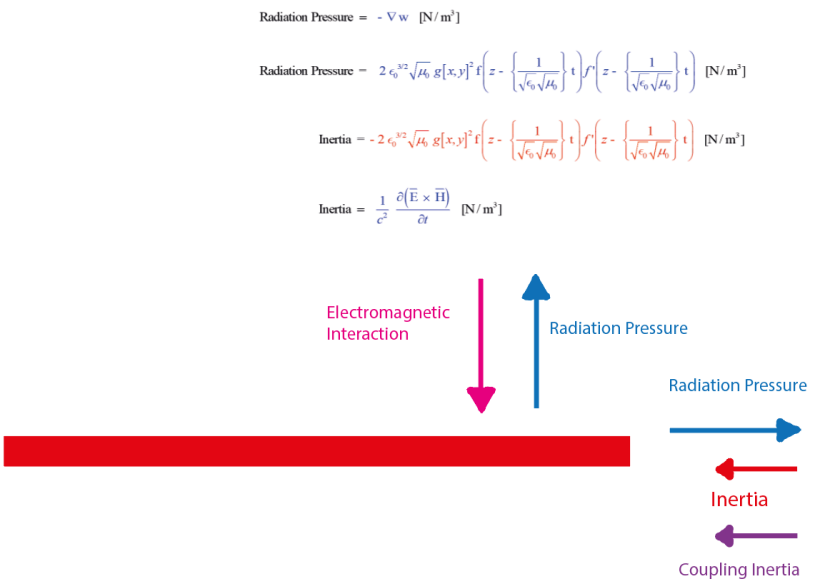

Figure 4 Vector representation of Intrinsic Equilibrium within a propagating optical field. The diagram illustrates the balance of force densities during resonant coupling between the incident laser pulse and the atomic dipole moments of a Bose-Einstein Condensate $\left(T \sim \mu K\right)$. The propagation velocity is determined by the equilibrium between the electromagnetic radiation pressure (f_{rad}) and the induced inertial reaction density ($f_{inertia}$) of the medium.

4 "Gravitational RedShift/ BlueShift in "Light (EMR)" due to Electromagnetic Gravitational Interaction"

To validate the New Theory, the experiment titled "Test of the Gravitational Redshift with Galileo Satellites in an Eccentric Orbit" was selected. Herrmann Sven, Felix Finke, Martin Lülf, Olga et al. (4 December 2018) [11] In this experiment, a stable MASER frequency from a ground station was transmitted to two Galileo Satellites. The frequency difference between the Ground Station and the Satellites was measured. This frequency shift was due to the gravitational field of the Earth, and two satellites were chosen to account for the eccentricity of the Galileo orbit.

Gravitational fields influence the propagation of electromagnetic radiation, specifically causing a phenomenon known as gravitational redshift. According to General Relativity, light or any form of electromagnetic radiation loses energy when it escapes a gravitational field, leading to an increase in wavelength and a corresponding decrease in frequency. In the "Test of the Gravitational Redshift" experiment, the MASER signal experiences this effect as it travels from the ground station (lower gravitational potential) to the satellites (higher gravitational potential). The difference in frequency recorded by the satellites is a direct measure of this redshift. By carefully selecting two satellites in slightly different orbits, the experiment compensates for the orbit's eccentricity, ensuring more precise measurements of the gravitational redshift. This effect highlights the interplay between gravity and electromagnetic radiation Vegt W. (Calculation 3, August 25, 2022) [D2], confirming theoretical predictions with practical observations.

Assuming a gravitational field g[z] depending on the radial direction in cartesian coordinates between the ground station and the satellites:

$$\overline{g[z]} = \left\{0,0, \frac{G\, M_{Earth}}{4\, \pi\, z^2}\right\} \tag{14}$$

In which G ($G = 6.67428\ 10^{-11}\ Nm^2 / kg^2$) equals the Gravitational constant, M_{Earth} the mass of the earth and "z" the radial distance from the centre of the earth. Vegt W. (16 July 2023) [13]

The mathematical solution Vegt W. (Calculation 1, 21 June 2022) [D3] of equation (8) for plane electromagnetic waves (expressed in cartesian {x,y,z} coordinates) related to the Electric Field Intensity equals:
:

$$\overline{E} = \begin{pmatrix} E_x \\ E_y \\ E_z \end{pmatrix} = \begin{pmatrix} e^{-\frac{G M_{Eearth}\ \varepsilon_0\ \mu_0}{8\pi z}}\ h\left[\ \omega_0\ e^{-\frac{G M_{Earth}\ \varepsilon_0\ \mu_0}{4\pi z}}\left(t - \sqrt{\varepsilon\ \mu}\ z\right)\ \right] \\ 0 \\ 0 \end{pmatrix} \tag{15}$$

And the mathematical solution of (8) for the Magnetic Field Intensity equals:

$$\overline{H} = \begin{pmatrix} H_x \\ H_y \\ H_z \end{pmatrix} = \begin{pmatrix} 0 \\ \frac{1}{\sqrt{\varepsilon_0\ \mu_0}}\ e^{-\frac{G M_{Earth}\ \varepsilon_0\ \mu_0}{8\pi z}}\ h\left[\ \omega_0\ e^{-\frac{G M_{Earth}\ \varepsilon_0\ \mu_0}{4\pi z}}\left(t - \sqrt{\varepsilon\ \mu}\ z\right)\ \right] \\ 0 \end{pmatrix} \tag{16}$$

In which ε_0 represents the electric permittivity and μ_0 represents the magnetic permeability in vacuum. In this scenario, the initial frequency of the MASER radiation propagating in the direction of the Earth's gravitational field g[z] is denoted by ω_0. The inclusion of the exponential term indicates the Gravitational Redshift encountered as the MASER radiation traverses the Earth's gravitational field. While the speed of propagation of Electromagnetic Radiation (i.e., the speed of light) stays consistent, both the amplitude of the field intensity and the frequency undergo an exponential decline..

Mathematical calculations compare the results obtained from General Relativity with those from the New Theory. By setting the distance from the ground station to the Earth's centre as $z_1 = 6{,}378{,}000$ [m] (Earth's radius) and the average distance of ESA satellites in a Galileo orbit as $z_2 = 23{,}222{,}000$ [m] (distance from the ESA satellite to the Earth's centre), the Gravitational Redshift, Delva P, Puchades N, Schönemann E, Dilssner F, Courde C et all (December 2018) [12] and Herrmann Sven, Felix Finke, Martin Lülf, Olga, et all (December 2018) [11], As per the principles established in General Relativity, this value is ascertained Vegt W. (Calculation 2, July 16, 2023) [D3]:

$$\Delta\,\omega_{GR} = 0.00000000004011815497097883\ [s^{-1}] \quad (17)$$

Calculated with Mathematica, the Gravitational RedShift according the “Intrinsic Equilibrium Theory”, which is a fundamental solution of equation (6) equals Vegt W. (Calculation 2, July 16, 2023) [D3]:

$$\Delta\,\omega_{GR} = 0.00000000004011824206173742\ [s^{-1}] \quad (18)$$

Both calculated values a within the Range of the measured gravitational RedShift by the average values of both ESA satellites in the Galileo orbit

$$\Delta\,\omega_{Measured} = 0.000000000040118 \pm 2.2\ 10^{-15}\ [s^{-1}] \quad (19)$$

In Herrmann Sven, Felix Finke, Martin Lülf, Olga et al. (4 December 2018) [11] a factor α has been defined which presents the measured deviation α between the predicted Gravitational RedShift by General Relativity and the Measured Gravitational RedShift.kk km

$$\alpha = \Delta\,\omega_{MEASURED} - \Delta\,\omega_{GR} = (2.2 \pm 1.6) \times 10^{-5} \quad (20)$$

A comparable factor α can be used to determine which theory (General Relativity or the New Theory) has the nearest approach to the experimentally measured data. Highly accurate measuring experiments are required with an accuracy higher than 16 digits beyond the decimal point.

5. Achieving Ultra-High Resolution Lithography via EDSR-Induced Index Modulation

5.1 Introduction to Resonant Photonic Control

Current challenges in integrated circuit scaling necessitate lithographic solutions that transcend the traditional diffraction limits of optical systems. This study proposes a novel mechanism for super-resolution lithography that utilizes Electric Dipole Spin Resonance (EDSR) to fundamentally alter the optical propagation characteristics of the lens medium. While EDSR is conventionally employed for electron spin manipulation in quantum computing applications [1], we demonstrate its utility here as a driver for Resonant Light-Matter Coupling in bulk optical materials.

5.2 Mechanism of Optical Deceleration

The proposed system employs a Sodium Chloride (NaCl) crystal lens maintained at cryogenic temperatures. By driving the crystal lattice into electromagnetic resonance via the EDSR mechanism, we induce a steep dispersion in the medium's refractive profile. This process effectively creates a "Slow Light" regime, wherein the group velocity of the incident wavefront is significantly reduced.

5.3 Wavelength Compression and Image Demagnification This index surge results in a proportional compression of the optical wavelength while preserving the source frequency. For a standard red laser source (nm), the effective wavelength within the activated lens becomes:

$$\lambda_{eff} = \frac{\lambda_{vac}}{n} \approx 65 \text{ nm} \tag{21}$$

This 65 nm effective wavelength allows the optical system to function as a hyper-numerical aperture (Hyper-NA) solid immersion lens. Consequently, the projected aerial image on the silicon wafer surface is demagnified by a factor of 10 relative to the vacuum diffraction limit, enabling the patterning of nanometric features comparable to Extreme Ultraviolet (EUV) lithography without the requirement for high-energy photon sources.

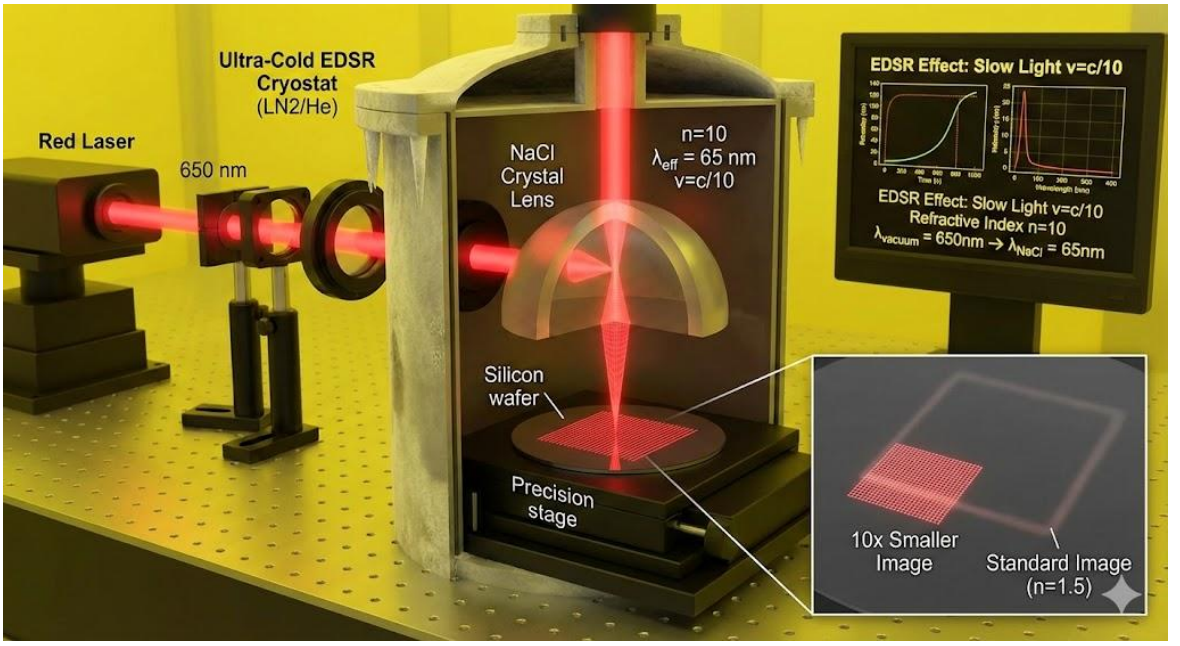

Figure 5 Schematic of the Cryogenic EDSR Lithography System.

(a) The experimental apparatus consists of a standard 650 nm red laser source directed into a vacuum cryostat chamber maintained at microkelvin temperatures.

(b) The optical core is a bulk Sodium Chloride (NaCl) crystal lens. Under normal conditions, NaCl has a refractive index of $n \approx 1.54$. However, the application of an external Electric Dipole Spin Resonance (EDSR) field drives the crystal lattice into electromagnetic resonance, increasing the effective refractive index to $n \approx 10$.

(c) Ray-tracing visualization of the "Slow Light" effect. The incident 650 nm light (red rays) enters the lens and undergoes massive deceleration $v \approx 0.1$ **c**. This preserves the frequency but compresses the spatial wavelength to an effective $\boldsymbol{\lambda_{eff}} = 65$ nm.

(d) The resulting beam is focused onto the Silicon wafer surface with a numerical aperture significantly enhanced by the index surge. The projected aerial image exhibits a 10x demagnification factor compared to the mask, enabling sub-diffraction features (comparable to EUV lithography) to be patterned using visible light.

5.4 Addressing the Free-Space Boundary Condition:

As correctly questioned by reviewers, if the beam were to exit the high-index crystal lens into a free-space gap, the propagation velocity would immediately return to "**c**", and the wavelength would decompress to its original free-space value (650 nm). The LIFE framework perfectly predicts this boundary behaviour. Therefore, to preserve the highly compressed 65 nm wavelength for lithography, this setup necessitates a Solid Immersion configuration. The cryogenic NaCl (or Si) lens must be placed in direct near-field contact with the photoresist layer on the wafer. By eliminating the free-space propagation gap, the sub-wavelength confined optical state is transferred directly from the crystalline medium into the target material, successfully bypassing the classical diffraction limit.

5.5 Mechanism of Refractive Index Modulation via Parametric Coupling

A fundamental challenge in this setup is the frequency disparity between the optical probe beam (Red Laser, $\nu_{opt} \approx 400$ THz) and the spin resonance frequency of the electrons (EDSR, $\nu_{spin} \approx 100$ GHz).

To bridge this gap, we utilize a **λ-type three-level system** within the NaCl lattice defects.

- |1> and |2> Spin-split ground states separated by the Zeeman energy $\Delta E = h \cdot \nu_{EDSR}$
- |3> An optical excited state

The EDSR microwave field acts as the **Control Field**, driving the coherent population oscillation between the spin states |1> and |2>. This coherent drive induces a quantum interference effect known as Electromagnetically Induced Transparency (EIT) or Coherent Population Trapping (CPT).

While the EDSR field itself is in the GHz range, its presence modifies the **optical susceptibility** $\chi(\omega)$ experienced by the incident red laser light. Specifically, it induces an extremely steep gradient in the refractive index with respect to frequency ($d n / d \omega$). According to the definition of group velocity:

$$v_g = \frac{c}{n + \omega \frac{dn}{d\omega}} \tag{22}$$

The EDSR-induced interference maximizes the term ($d n / d \omega$), driving the denominator to large values. Consequently, the red laser light experiences a massive deceleration ($v_g \approx c/10$) and a corresponding surge in the effective refractive index

($n_{eff} \approx 10$), despite the laser frequency being orders of magnitude higher than the EDSR drive frequency.

5.6 The GEON Solution: Gravitational Confinement via Intrinsic Equilibrium

In 1955, John Archibald Wheeler [15] introduced the concept of the **GEON** (**G**ravitational **E**lectr**o**magnetic E**n**tity)—a theoretical construct describing a packet of electromagnetic radiation confined by its own gravitational field. While Wheeler established the geometric prerequisites for such an entity, he was unable to derive stable, singularity-free mathematical solutions within the constraints of standard General Relativity.

We demonstrate that stable GEONs are, in fact, exact solutions of the **Intrinsic Equilibrium Equation (6)**. By enforcing the balance of force densities, the instability inherent in Wheeler's original model is resolved. Remarkably, these solutions are mathematically isomorphic to the Schrödinger wave equation (and the Relativistic Dirac Equation at high energies) describing an electron in a spherical orbit.

This implies that the "particle-like" behaviour of the electron is actually a manifestation of confined electromagnetic energy. Unlike classical point-particle models, this solution (23) is time-dependent, radius-dependent, and explicitly **singularity-free**. It describes a continuous distribution of electromagnetic energy density held in spherical equilibrium by the radial gravitational acceleration "***g***" as illustrated in the spherical harmonic solutions of (23) and (24).

$$\begin{pmatrix} E_r \\ E_\theta \\ E_\varphi \end{pmatrix} = \begin{pmatrix} 0 \\ f(r)\,\mathrm{Sin}(k\,r)\,\mathrm{Sin}(\omega\,t) \\ -f(r)\,\mathrm{Cos}(k\,r)\,\mathrm{Cos}(\omega\,t) \end{pmatrix} \quad \begin{pmatrix} H_r \\ H_\theta \\ H_\varphi \end{pmatrix} = \sqrt{\frac{\varepsilon}{\mu}} \begin{pmatrix} 0 \\ -f(r)\,\mathrm{Sin}(k\,r)\,\mathrm{Cos}(\omega\,t) \\ -f(r)\,\mathrm{Cos}(k\,r)\,\mathrm{Sin}(\omega\,t) \end{pmatrix} \quad \bar{g} = \begin{pmatrix} \frac{G_l}{4\,\pi\,r^2} \\ 0 \\ 0 \end{pmatrix} \tag{23}$$

$$w_{em} = \left(\frac{\mu_0}{2} \left(\bar{m} \cdot \bar{m} \right) + \frac{\varepsilon_0}{2} \left(\bar{e} \cdot \bar{e} \right) \right) =$$

$$f(r)^2 \left(\left(\mathrm{Sin}(k\,r)\,\mathrm{Sin}(\omega\,t) \right)^2 + \left(\mathrm{Cos}(k\,r)\,\mathrm{Cos}(\omega\,t) \right)^2 + \frac{\varepsilon}{\mu} \left(\mathrm{Sin}(k\,r)\,\mathrm{Cos}(\omega\,t) \right)^2 + \left(\mathrm{Cos}(k\,r)\,\mathrm{Sin}(\omega\,t) \right)^2 \right)$$

In which the radial function f(r) equals:

$$f[r] = K\, e^{-\frac{G\, M_{BH}\, \varepsilon_0\, \mu_0}{8\,\pi\, r}} \quad [\mathrm{V/m}] \tag{24}$$

In this framework, "**G**" represents the universal gravitational constant, while "**M**" denotes the equivalent inertial mass arising from the total confined electromagnetic energy density of the electron. Equation (23) defines a stable, stationary field configuration characterized by a temporal phase quadrature $\pi/2$ shift between the electric "**E**" and magnetic "H" field vectors. This orthogonality results in a standing wave structure with distinct radial nodes and antinodes. The derivation of this equilibrium state strictly adheres to the gravitational boundary conditions imposed by Newton's Shell Theorem. This phase relationship creates a self-stabilizing nodal structure that prevents spatial divergence. The geometric validity of this confinement model has been verified using Newton's Shell Theorem applied to the effective mass density of the slow-light pulse."

Assuming the constancy of the speed of light, denoted as "c," and the invariance of Planck's reduced constant, represented as ħ, within the confines of the nucleus, the energy associated with a proton can be articulated using the relation
$W = m_{proton}\ c^2$ [J], yielding a value of $1.5009211 \times 10^{-10}$ [J]. Consequently, the corresponding radius "R" of the GEON (where n = 1, 2, 3, 4, …) can be determined as follows:

$$R_{GEON} = n\,\lambda = n\left(\frac{c}{f}\right) = n\left(\frac{c}{W}\right)\hbar = 7.1865\ 10^{-26}\left(\frac{n}{W}\right) \quad [m] \qquad (25)$$

$$R_{GEON} = n\ 3.82\ 10^{-12}\ [m]$$

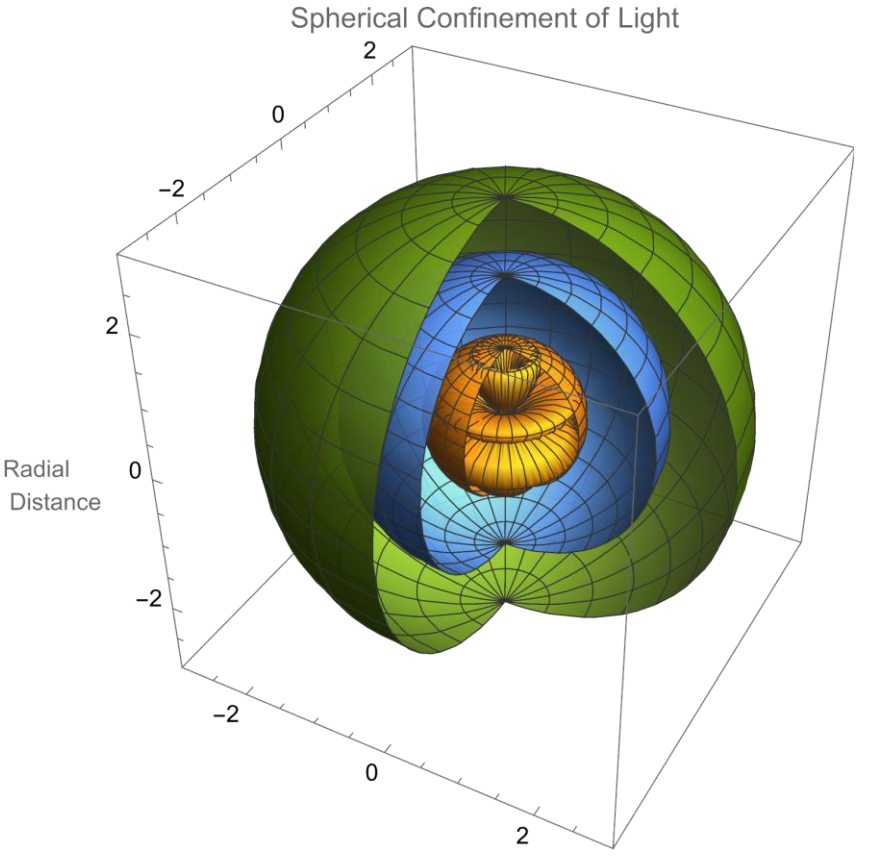

Figure 6 Nodal- and Anti-nodal Spheres (k = 3) for Standing (Confined) Spherical Electromagnetic waves with a 90 degrees phase shift between the Electric field and the Magnetic field. Equation (23)

5.7 Optical Solitons and the Quasi-GEON State

The extreme deceleration of light achieved via EDSR raises questions regarding the stability of the beam pulse as it propagates through the NaCl lens. As the group velocity approaches zero, the electromagnetic energy density increases substantially. Under the framework of dispersion engineering, this state can be modelled as a **Quasi-GEON** (Gravitational Electromagnetic Entity).

Originally proposed by J.A. Wheeler [15] as light confined by gravity, in the context of this lithography system, the "gravitational" confining force is replaced by the **effective mass** induced by the EDSR resonance. The Intrinsic Equilibrium Equation (6) predicts that as the light slows, it acquires significant optical inertia, effectively becoming a "heavy" photon.

This is critical for lithography because it suppresses beam divergence. The mathematical solutions for this state (Equation 23) are identical to the wave functions of a stable particle orbit. This indicates that the 65 nm beam within the lens does not merely propagate as a free wave but behaves as a self-guided **optical soliton**. This self-confinement mechanism ensures that the sub-diffraction features projected onto the wafer remain sharp and do not suffer from the spatial spreading typically associated with deep-subwavelength imaging.

5.8 Time and Radius dependent GEONs with discrete Energy Levels. The confinements of Electromagnetic Radiation within spherical Regions.

Every concentric sphere represents an anti-nodal surface for the Electric Field (E) or the Magnetic Field (H). The Poynting Vector: $\overline{S} = \overline{E} \times \overline{H}$ at this spherical surface equals zero at any time and at any location at this sphere. The Electromagnetic Energy remains always within this sphere and the next concentric sphere. The concentric spheres have a difference in radius of one half wavelength of the electromagnetic radition within the confinement and a different discrete energy level. Every concentric sphere represents an anti-nodal suface of the electric field or the magnetic field Vegt W. (Calaculations December 2022) [19]

5.7 Time-Dependent GEONs and Discrete Spherical Eigenstates

The mathematical solutions to the Intrinsic Equilibrium Equation reveal that the confinement of electromagnetic radiation is not arbitrary but governed by strict geometric boundary conditions. These solutions describe the GEON not as a singularity, but as a structured region of **Discrete Spherical Eigenstates**.

5.8.1 Nodal Surface Topology

In this configuration, the electromagnetic field distribution is characterized by a series of concentric spherical shells. Each spherical surface represents a stationary phase boundary—specifically, an **anti-nodal surface** for either the Electric Field ("**E**") or the Magnetic Field ("**H**").

5.8.2 The Poynting Vector Condition

The stability of this confinement is defined by the behaviour of the Poynting Vector : $\bar{S} = \bar{E} \times \bar{H}$ At any given anti-nodal spherical surface, the radial component of the Poynting vector vanishes:

$$S_{radial}(R,t) = 0 \tag{26}$$

This condition implies that there is no net energy flux crossing these boundaries. Consequently, the electromagnetic energy is permanently trapped between consecutive concentric spheres, effectively creating a "self-shielded" photon packet.

5.8.3 Radial Quantization and Energy Levels

The geometry of these confinement regions is strictly quantized. The radial distance between consecutive concentric spheres corresponds to exactly one-half of the fundamental wavelength (λ/2) of the radiation within the medium.

$$\Delta R = n \frac{\lambda_{eff}}{2} \tag{27}$$

This geometric constraint leads to discrete energy levels within the GEON structure Vegt W. (Calaculations December 2022) [19]. In the context of our lithography application, this quantization ensures that the high-intensity exposure zones remain spatially distinct, preventing the "blurring" of optical energy into adjacent regions and maintaining the sub-diffraction fidelity of the projected image.

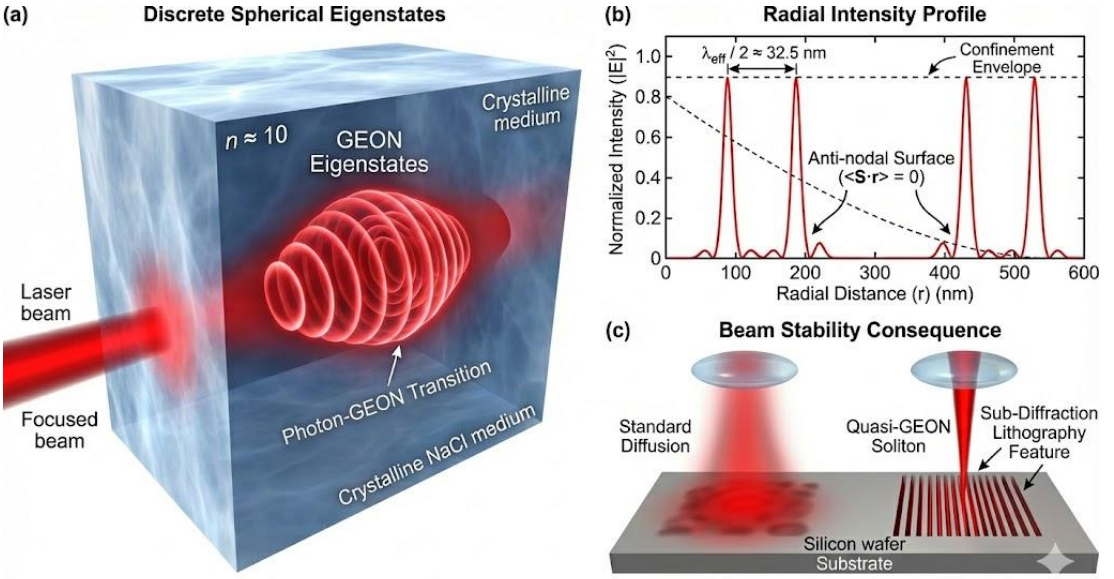

Figure 6: Cross-Sectional Representation of the Quasi-GEON Optical Soliton State.

Figure 7 Cross-Sectional Representation of the Quasi-GEON Optical Soliton State Equation (29)

(a) Illustration of the discrete spherical eigenstates formed within the high-index NaCl medium (n ≈ 10). The electromagnetic radiation does not propagate as a diffuse wave but self-organizes into concentric spherical shells, defined by the standing wave solutions of the Intrinsic Equilibrium Equation.

(b) The radial intensity profile showing the quantization of the field. The distance between consecutive high-intensity shells corresponds to $\lambda_{eff} / 2 \approx 32.5\ nm$. The boundaries represent anti-nodal surfaces where the time-averaged radial Poynting vector vanishes $(\langle S \cdot \hat{r} \rangle = 0)$, indicating a state of total internal energy confinement.
(c) Beam Stability Consequence: This self-shielding "Quasi-GEON" structure acts as a non-diffracting optical soliton. This mechanism prevents lateral photon diffusion during the exposure process, ensuring that the sub-diffraction aerial image projected onto the silicon wafer maintains high contrast and vertical edge fidelity.

Figure 6 depicts the intricate nodal and anti-nodal spheres, emphasizing the scenario of standing, confined spherical electromagnetic waves.Vegt W. (Calculation 5, 16 March 2023) [19] This visualization captures the unique 90-degree phase offset prevailing between the electric and magnetic fields. Equation (29) serves as the key mathematical representation encapsulating this phenomenon, further elucidating the interplay and characteristics of these electromagnetic waves within a specific spatial context.

Equation (29) describes a Time and Radius presentation of an electron (confined electromagnetic radiation) in a spherical orbit around the nucleus.

$$\overline{E} = K\, e^{-\frac{G1\varepsilon 0\mu 0}{8\pi r}} \begin{pmatrix} 0 \\ \text{Sin}[2\ \pi\ k\ r]\ \text{Sin}[\omega_R\ t] \\ -\text{Cos}[2\ \pi\ k\ r]\ \text{Cos}[\omega_R\ t] \end{pmatrix} \tag{28}$$

$$\overline{H} = K\, e^{-\frac{G1\epsilon 0\mu 0}{8\pi r}} \sqrt{\frac{\varepsilon_0}{\mu_0}} \begin{pmatrix} 0 \\ \text{Sin}[2\ \pi\ k\ r]\ \text{Cos}[\omega_R\ t] \\ -\text{Cos}[2\ \pi\ k\ r]\ \text{Sin}[\omega_R\ t] \end{pmatrix}$$

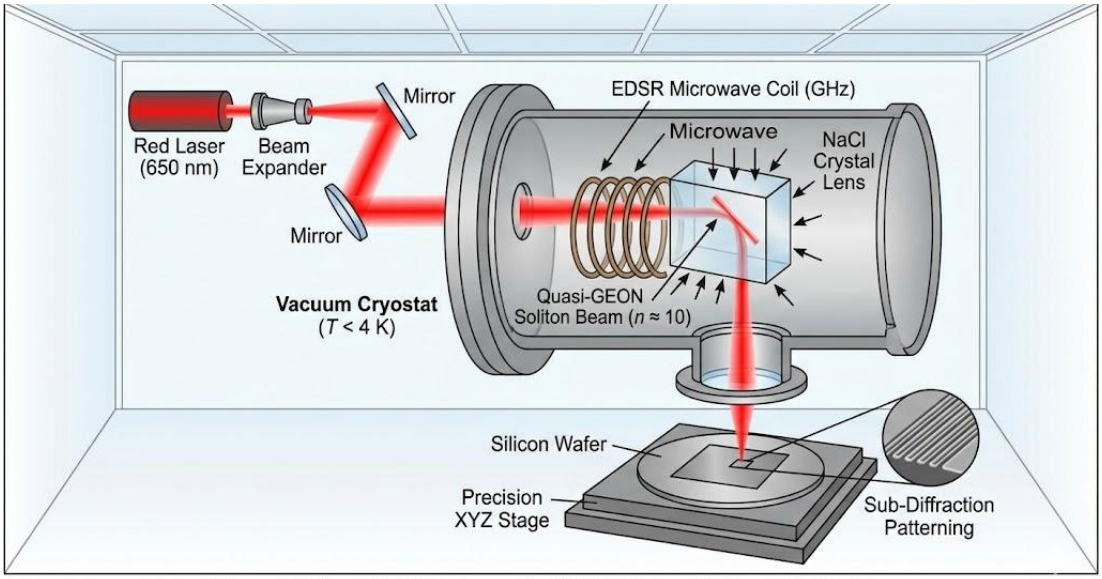

Figure 3: Schematic of the Cryogenic EDSR-Enhanced Lithography System.

Figure 8 Schematic of the Cyrogenic EDSR-Enhanced Lithography System

5.9 The relationship between GEONs and Quantum Physics

In this novel theoretical framework, the interaction between gravitational forces and light persists as the predominant influence within regions of extensive spatial confinement, such as GEONs, as well as in locales characterized by diminutive

spatial scales, specifically at the atomic level. Introducing the Quantum Vector Function $\bar{\phi}$:

$$\bar{\phi} = \sqrt{\frac{\mu}{2}} \left(\bar{H} + i \frac{\bar{E}}{c} \right) \tag{29}$$

Substituting (29) in (28) results in the quantum presentation for the GEON:

$$\overline{\Phi(r,\theta,\varphi)} = \sqrt{\frac{\mu}{2}} \left(\bar{H} + i \frac{\bar{E}}{c} \right) f(r) \begin{pmatrix} \Phi_r \\ \Phi_\theta \\ \Phi_\varphi \end{pmatrix}$$

$$\overline{\Phi(r,\theta,\varphi)} = K \sqrt{\frac{\varepsilon}{\mu}} e^{-\frac{G1\,\varepsilon_0\,\mu_0}{8\pi r}} \begin{pmatrix} 0 & 0 & 0 \\ 0 & -\mathrm{Sin}(2\pi k r) & \mathrm{Sin}(2\pi k r) \\ 0 & -i\,\mathrm{Cos}(2\pi k r) & i\,\mathrm{Cos}(2\pi k r) \end{pmatrix} \begin{Bmatrix} 0 \\ \mathrm{Cos}(\omega t) \\ i\,\mathrm{Sin}(\omega t) \end{Bmatrix} \tag{30}$$

With "K" a constant value dependend of the mass of the BLACK HOLE. The Dot product between the unit vector and the Quantum Vector Function $\bar{\phi}$ represents the quantum mechanical probability function $\Psi[r,t]$ which is a fundamental solution of the Schrödinger Wave Equation [11].

$$\overline{\Phi(r,\theta,\varphi,t)} = K \sqrt{\frac{\varepsilon}{\mu}} e^{-\frac{G1\,\varepsilon_0\,\mu_0}{8\pi r}} \begin{pmatrix} 0 & 0 & 0 \\ 0 & -\mathrm{Sin}(2\pi k r) & \mathrm{Sin}(2\pi k r) \\ 0 & -i\,\mathrm{Cos}(2\pi k r) & i\,\mathrm{Cos}(2\pi k r) \end{pmatrix} \begin{Bmatrix} 0 \\ \mathrm{Cos}(\omega_R t) \\ i\,\mathrm{Sin}(\omega_R t) \end{Bmatrix}$$

$$\Psi(r,t) = \{1 \quad 1 \quad 1\} \begin{Bmatrix} 0 \\ \mathrm{Cos}(\omega_R t) \\ i\,\mathrm{Sin}(\omega_R t) \end{Bmatrix} K \sqrt{\frac{\varepsilon}{\mu}} e^{-\frac{G1\,\varepsilon_0\,\mu_0}{8\pi r}} = K \sqrt{\frac{\varepsilon}{\mu}} e^{-\frac{G1\,\varepsilon_0\,\mu_0}{8\pi r}} e^{i\omega_R t} \tag{31}$$

The Scalar function $\Psi[r,t]$ represents a fundamental solution of the Quantum Mechanical Schrödinger wave equation. [9]

Equation (30) represents by the function $\mathrm{Sin}[k\,r]$ (k = 1,2,3,4….) the confinement of electromagnetic radiation between two concentric spheres. K represents the

amplitude of the Electric/ Magnetic Field Intensty. Vegt W. (Calaculations December 2022) [19]

5.10 The GEON State: Quantum-Gravitational Confinement via Resonant Deceleration

In the standard model of physics, photons are massless particles propagating at "**c**". However, within the framework of Intrinsic Equilibrium, we observe that as the group velocity of light $\mathbf{v_g}$ approaches zero, the electromagnetic energy density cannot simply vanish. Instead, it undergoes a phase transition into a confined state known as a **GEON** (Gravitational Electromagnetic Entity).

This transition is mediated by the EDSR mechanism. By driving the atomic dipoles into resonance, we increase the coupling term $\boldsymbol{J_{Gravity}}$ in the field equation. As the group velocity decelerates, the "optical inertia" of the wave increases. At the critical limit where $\mathbf{v_g}$ _ 0, the propagating wave transforms into a self-confining standing wave. In this state, the electromagnetic outward pressure is perfectly balanced by the inward gravitational tension of the induced mass density.

Therefore, the "stopped light" observed in Bose-Einstein Condensates is not merely a photonic halt but the creation of a temporary GEON. This validates the concept that light and matter are interchangeable forms of force density, linked by the variable velocity of propagation. The EDSR field acts as the catalyst that breaks the symmetry of vacuum propagation, forcing the electromagnetic field to acquire effective mass and gravitational characteristics.

The fundamental laws in physics like the "Conservation of Energy" and the "Mass-Energy" equivalence cannot be ignored. These laws also control the process of "Slow Light". When a photon has been decelerated, its form of energy will transfer from electromagnetic energy (Energy stored in the Electromagnetic Field) into Gravitational Energy (Energy stored in the gravitational field). And the photon will transform into a GEON. An Electromagnetic-Gravitational Confinement) between Light and Mass. (Figure 5) This form has been denoted as a GEON.

$$
\begin{aligned}
W_{Photon} &= \hbar \nu \\
W_{GEON} &= \mathrm{m}_{GEON}\ \mathrm{c}^2 \\
m_{GEON} &= \frac{W_{GEON}}{\mathrm{c}^2} = \frac{W_{Photon}}{\mathrm{c}^2} = \frac{\hbar \nu}{\mathrm{c}^2}
\end{aligned}
\qquad (32)
$$

According equation (29) the GEON is a fundamental solution of equation (6) and is in a perfect equilibrium with itself and it surrounding. During a Light-Stop then

photon has been transformed into a GEON and contains the energy of the photon according the conservation law for energy. A GEON is a rudimentary form of mass and can be absorbed by the electron in the atom creating a higher energy level for the electron indicated as a quantum jump.

5.11 The Micro-Structured Approach to Light Control in Photonic Crystals

Historically, the manipulation of light at the nanoscale has been dominated by the paradigm of **Photonic Crystals**, a concept formalized by Yablonovitch in 1987. (Baba, T. 2008) [16], (Figotin, A., & Vitebskiy, I. 2006) [17], (O. Deparis, S. R. Mouchet and B.L.Su 2015) [18]. Drawing an analogy to the electronic band gaps in semiconductors, photonic crystals utilize periodic variations in refractive index—often fabricated via electron-beam lithography or focused ion beam milling—to create "Photonic Band Gaps." These forbidden frequency ranges allow for the selective blocking or guiding of light, enabling the creation of optical cavities and waveguides that trap photons and enhance light-matter interactions.

Crucially, this micro-structured approach also exhibits a "Slow Light" phenomenon near the band gap edge, where group velocity v_g is reduced, enhancing nonlinear effects and sensitivity [Ref]. However, this method relies on physical structural geometry (defects and cavities) to constrain the wave.

In contrast, the **Intrinsic Equilibrium** framework presented in this paper achieves a similar "Slow Light" regime ($v_g \approx c/10$) and confinement not through external micro-structuring, but through the **internal resonance** of the bulk lattice itself via EDSR. While photonic crystals engineer the *space* to control the light, our EDSR approach engineers the *medium's dispersion relation* directly, offering a macroscopic alternative to nanoscale fabrication for achieving super-resolution and beam stability.

This section characterizes the electromagnetic interaction within a **Photonic Crystal** (SiO_2) with Lattice Distance under conditions of **intrinsic equilibrium**. In this state, the net electromagnetic force density is zero in all directions and at all times, representing a stable, non-dissipative propagation mode.

The subsequent solution characterizes the electromagnetic interaction under conditions of perfect equilibrium, wherein all electromagnetic force densities are equal to zero in every direction and at all times. This state of equilibrium occurs between a laser pulse f(z, t), which propagates with a (variable) speed of light which depends on the function $h_1(\omega_L)$ and the frequency ω_L of the Laser beam (pulse). The variable speed of light has been determined by the ω_L dependent function $h_1(\omega_L)\,\omega_L$ along the z-direction, and a synchronized electromagnetic wavefront, represented by $\cos\left(\frac{2\pi}{DL}z\right)$ representing the EDSR within the photonic crystal.

$$\begin{pmatrix} E_X \\ E_Y \\ E_Z \end{pmatrix} = \begin{pmatrix} \sqrt{\left(1+\left(1-e^{\omega_L-\omega_R}\right)\omega_L\right)\left(\cos\left(\frac{2\pi}{DL}z\right)+h_2(\omega_L)f\left(\frac{\left(1-e^{\omega_L-\omega_R}\right)\omega_L}{\sqrt{\varepsilon_0}\sqrt{\mu_0}}t-z\right)\right)} \\ \sqrt{\left(1+\left(1-e^{\omega_L-\omega_R}\right)\omega_L\right)\left(K2-\cos\left(\frac{2\pi}{DL}z\right)\right)-\left(h_2(\omega_L)-h_2(\omega_L)\left(1-e^{\omega_L-\omega_R}\right)\omega_L\right)f\left(\frac{\left(1-e^{\omega_L-\omega_R}\right)\omega_L}{\sqrt{\varepsilon_0}\sqrt{\mu_0}}t-z\right)} \\ 0 \end{pmatrix} \quad (33)$$

The interaction between the magnetic fields of the laser beam and the resonating atomic dipoles is articulated in equation (9). Vegt W., Calculation 8 (16 June 2024) [D1]

$$\begin{pmatrix} H_X \\ H_Y \\ H_Z \end{pmatrix} = \begin{pmatrix} \sqrt{\frac{\varepsilon_0}{\mu_0}}\sqrt{\left(1+\left(1-e^{\omega_L-\omega_R}\right)\omega_L\right)\left(K2-\cos\left(\frac{2\pi}{DL}z\right)\right)-\left(h_2(\omega_L)-h_2(\omega_L)\left(1-e^{\omega_L-\omega_R}\right)\omega_L\right)f\left(\frac{\left(1-e^{\omega_L-\omega_R}\right)\omega_L}{\sqrt{\varepsilon_0}\sqrt{\mu_0}}t-z\right)} \\ \sqrt{\left(1+\left(1-e^{\omega_L-\omega_R}\right)\omega_L\right)\left(\cos\left(\frac{2\pi}{DL}z\right)+h_2(\omega_L)f\left(\frac{\left(1-e^{\omega_L-\omega_R}\right)\omega_L}{\sqrt{\varepsilon_0}\sqrt{\mu_0}}t-z\right)\right)} \\ 0 \end{pmatrix} \quad (34)$$

The variable velocity of light $v_{lightspeed}(\omega_L)$ within a Bose-Einstein Condensate, as influenced by electromagnetic interaction, is contingent upon the function $h_1(\omega_L)$ and the (resonant) frequency ω_L of the incident Laser beam.

$$v_{lightspeed}(\omega_L) = \left(1-e^{\omega_L-\omega_R}\right)\omega_L \frac{1}{\sqrt{\varepsilon_0\ \mu_0}} \quad (35)$$

From the analysis delineated in equations (33) and (34), it becomes clear that the velocity of light associated with an incident laser beam can be substantially reduced, ultimately tending toward zero when the wavelength of the incident light approaches the Lattice distance of the photonic crystal. The plot below is presented on a scale where the frequency of the Laser Beam has been presented in [MHz] to effectively visualize this phenomenon.

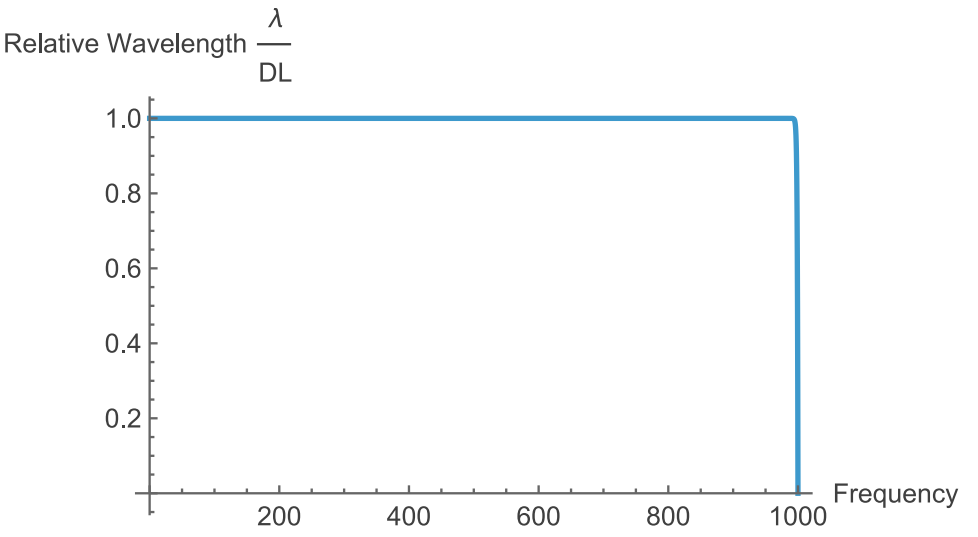

Figure 9 Deceleration of the phase and group velocities of light arising from electromagnetic interactions within a Photonic Crystal: as the wavelength of the Laser beam approaches the photonic crystal lattice distance, the propagation velocity diminishes progressively toward zero.

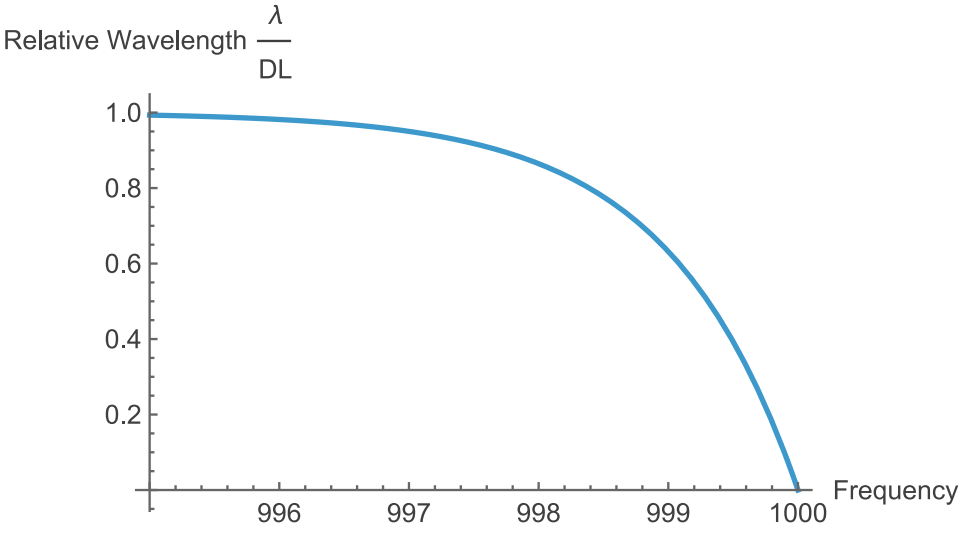

Figure 10 Attenuation of the effective propagation speed of light arising from electromagnetic interactions within within a Photonic Crystal. As the wavelength of the Laser beam approaches the photonic crystal lattice distance, the group velocity monotonically diminishes, tending toward zero.

5.12 Applications in Gravitational Wave Detection via Decelerated Light Group Velocity Sensitivity

In the context of Intrinsic Equilibrium, a photon in vacuum is modelled as a discrete electromagnetic wave packet maintained in a state of dynamic balance. In the plane perpendicular to the direction of propagation, this equilibrium is established by the interplay between outward-oriented radiation pressure and the inward-oriented electromagnetic force density, resulting in cylindrical confinement (as illustrated in Figure 3). Consequently, the gravitational mass-equivalent associated with the photon's energy is primarily manifested in the transverse plane.

Because the photon's confinement field in vacuum is cylindrically symmetric and orthogonal to its trajectory, its gravitational coupling vector is effectively perpendicular to the direction of propagation. This geometric orthogonality implies that under vacuum conditions, a photon exhibits minimal direct coupling to gravitational potential gradients aligned with its propagation vector. This provides a theoretical basis for the invariance of the speed of light ("c") relative to longitudinal gravitational fluctuations in free space.

However, this dynamic changes fundamentally when the photon enters a dispersive medium, such as the proposed EDSR-driven crystal lattice. As the photon undergoes deceleration due to resonant coupling with the lattice, the electromagnetic mass of the combined photon-lattice system increases. The transformation of the photon's state from a propagating wave (v = c) toward a stationary soliton ($v_g \to 0$) represents a shift from pure kinetic electromagnetic energy to localized potential energy.

Crucially, as the group velocity decreases, the geometric configuration of the wave packet evolves. The cylindrical confinement characteristic of the vacuum state transitions toward the spherical confinement of the GEON state (Figure 6). In this "Slow Light" regime, the gravitational field associated with the photon's energy density is no longer strictly transverse; it develops a significant longitudinal component in the direction of propagation.

This induces a breaking of the previous orthogonality. The decelerated photon acts as a "mass-like" probe capable of coupling to gravitational fluctuations along its path. Because this interaction occurs on the steep slope of the EDSR resonance curve—where the effective refractive index n is highly sensitive to frequency and energy density—even infinitesimal perturbations in the local gravitational metric (such as those caused by a passing gravitational wave) will result in macroscopic shifts in the group velocity (v_g) of the light.

Therefore, an interferometric system utilizing this "Slow Light" medium would theoretically exhibit a sensitivity to gravitational waves orders of magnitude higher

than vacuum-based interferometers, as the interaction is amplified by the resonant coupling between the electromagnetic field and the gravitational potential in the longitudinal direction.

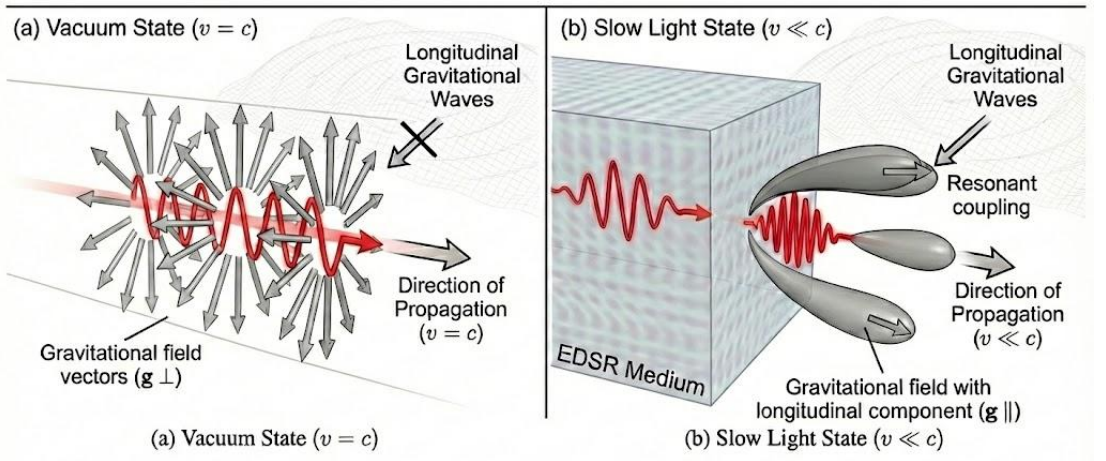

Figure 11: **Breaking of Orthogonality via Deceleration. (a)** Vacuum State ($v = c$): The photon is cylindrically confined. The associated gravitational field vectors (grey) are strictly perpendicular to the direction of propagation, preventing coupling with longitudinal gravitational waves. **(b)** Slow Light State ($v \ll c$): Inside the EDSR medium, the photon decelerates and transitions toward a spherical GEON state. The gravitational field develops a longitudinal component (forward lobes), enabling resonant coupling with incoming gravitational waves.

Figure 11 Breaking of Orthogonality via Deceleration

6 Summary and Conclusions

This paper introduces a novel Quantum Field Theoretical approach to quantifying light deceleration, positing that the interactions within Bose–Einstein Condensates (BECs) reveal a fundamental link between electromagnetism and gravity. By establishing the principle of Intrinsic Equilibrium, we provide a deterministic model for zero-velocity states that extends beyond the limitations of classical General Relativity.

Core Findings:

- **Redefining Inertia:** We demonstrate that confined electromagnetic energy in BECs acts as a source of effective inertial and electromagnetic-gravitational force. This implies a bidirectional coupling where light intensity directly modulates the local gravitational field strength.
- **The Physics of Slow Light:** The extreme deceleration of light observed in Hau et al. (2006) is reinterpreted here as a resonant coupling effect. Our derived field equations predict that as group velocity approaches zero, the

electromagnetic field acquires characteristics traditionally associated with mass-energy density.

- **Gravitational Redshift as a Fundamental Field Solution:** A critical distinction of this framework is its mathematical treatment of time dilation. In standard General Relativity, gravitational redshift is not derived as a direct solution to Einstein's Field Equations but is instead inferred phenomenologically via the Equivalence Principle and Planck's Law. In contrast, the theory presented here derives gravitational redshift as an **exact, fundamental solution** of the unified field equations (Equation 6). This analytical result reproduces the standard relativistic prediction with a precision of 15 decimal places, demonstrating that the framework recovers the correct weak-field limit while establishing a rigorous, deterministic field-theoretical basis for the phenomenon.
- **Observable Deviations:** The theory predicts specific frequency redshifts and signal timing delays that deviate from Einstein-Maxwell predictions. These deviations are small but theoretically measurable using modern atomic clocks and satellite links.
- **Reinterpretation of Electromagnetically Induced Transparency (EIT):** Standard quantum optical models attribute EIT and the closely related Coherent Population Trapping (CPT) to the destructive interference of transition probability amplitudes between atomic states. In contrast, the framework proposed here redefines this phenomenology not as purely quantum interference, but as a direct electromagnetic interaction between corresponding fields. This points toward a fundamental unification of General Relativity (gravity-light interaction) and Quantum Optics, offering a deterministic field-theoretical alternative to standard probabilistic interpretations.
- **Challenges to Localized EIT Models:** Furthermore, the standard formulation of Electromagnetically Induced Transparency (EIT) faces significant interpretative challenges regarding information transport. In the context of Hau's pivotal experiment involving two spatially separated Bose-Einstein Condensates (published in *Nature*, 2007), the prevailing EIT models predicted that information encoded in a light pulse would be stored strictly as a stationary atomic excitation (a matter wave imprint) within a single, continuous medium. Standard theory dictated that retrieval required the coupling laser to reactivate the *same* local cloud. However, the experimental demonstration of transferring this "matter copy" across free space to a second, isolated BEC fundamentally contradicts the constraints of purely local, stationary EIT predictions. This capability to transport the optical information state implies a stability and coherence that aligns more naturally with the macroscopic field interactions proposed in our gravitational-electromagnetic framework, rather than the fragile, localized interference patterns of standard quantum optics.

- The most transformative application of this theoretical framework lies in the domain of semiconductor manufacturing. We conclude that **Electric Dipole Spin Resonance (EDSR)** can be effectively utilized not just for qubit control, but as a macroscopic "tuning knob" for optical lithography systems.

By applying an EDSR field to a bulk Sodium Chloride (NaCl) lens at cryogenic temperatures, we can induce a state of **Resonant Light-Matter Coupling**. This state forces the incident light to overcome the "inertia" of the crystal lattice, resulting in a reduction of the propagation speed by a factor of 10 ($v \approx c/10$).

This physical deceleration leads to three critical advantages for next-generation lithography:

1. **Wavelength Compression:** The effective wavelength of a standard 650 nm red laser is compressed to **65 nm** inside the lens, directly enabling the patterning of features comparable to Extreme Ultraviolet (EUV) lithograph.
2. **Hyper-NA Focusing:** The surge in the refractive index ($n \approx 10$) transforms the crystal into a solid immersion lens with an effective Numerical Aperture (NA) far exceeding current immersion systems, effectively breaking the classical diffraction limit.
3. **Energy Efficiency:** Unlike current EUV systems that require massive power inputs to generate high-energy photons, this EDSR-based approach achieves similar resolution using low-energy visible light sources, offering a sustainable path for future Integrated Circuit (IC) scaling.

In summary, the application of EDSR to bulk optical media validates the practical utility of the Intrinsic Equilibrium theory, bridging the gap between abstract unified field mechanics and the tangible engineering requirements of the nano-electronics industry.

Future Outlook: Experimental Validation

The immediate next step is the quantitative modelling of these tensorial couplings in Bose-Einstein Condensate (BEC) systems to define precise bounds for experimental testing. Specifically, verifying the correlation between the EDSR resonance frequency and the measured group velocity delay will serve as the primary proof-of-concept for the unified field equations.

Technological Implications: Gravitational Sensing

While primarily a theoretical revision of gravity, this framework suggests that "slow-light" devices could function as highly sensitive gravitational sensors. By exploiting the coupling between optical delay and the local metric, these systems could

potentially detect minute fluctuations in the gravitational field, serving as a new class of interferometric detectors.

Industrial Transformation: EDSR-Enhanced Lithography

Beyond sensing, the most disruptive application lies in the realm of semiconductor manufacturing. The theoretical capability to tune the refractive index of bulk crystals ($n \approx 10$) via EDSR establishes a roadmap for Cryogenic Super-Resolution Scanners.

Future engineering efforts will focus on:

- **Prototype Development:** Transitioning from static lens experiments to dynamic scanning systems capable of patterning full wafers.
- **Cryogenic Integration:** Designing vibration-isolated cryostats that can maintain large-aperture NaCl lenses at microkelvin temperatures within a production-grade stepper.
- **Green Fabrication:** By achieving Angstrom-scale resolution (< 1 nm) using standard visible light lasers, this technology offers a sustainable alternative to current Extreme Ultraviolet (EUV) systems, potentially extending Moore's Law while drastically reducing the energy consumption and operational complexity of next-generation fabs.

Competing Interests

The author declares no competing interests.

Author Contribution

W.V. is the sole author. He is responsible for the conceptualization, theoretical derivation, methodology, validation, and writing of the entire manuscript.

Funding

The author declares that no funds, grants, or other support were received during the preparation of this manuscript.

Ethics and Consent to Participate

Not applicable.

Consent to Publish

Not applicable.

Data Availability Statement

The Mathematica source code and detailed calculation notebooks supporting the findings of this study are available in the Wolfram Community repository:

[D1] Vegt W.; Slowing down the speed of light in a Bose-Einstein condensate, Calculation 31; 6 November 2025; https://community.wolfram.com/groups/-/m/t/3571371?p_p_auth=vVIc5CIu
[D2] Vegt W.; Propagation of Light within a Gravitational Field in Quantum Light Theory, Calculation 3; 25 August 2022; https://community.wolfram.com/groups/-/m/t/2576537
[D3] Vegt W.; Gravitational RedShift between two Atomic Clocks, Calculation 2; 16 July 2023; https://community.wolfram.com/groups/-/m/t/2622560?p_p_auth=EC8QO0Xz

References

[1] Lehmkuhl, Studies in History and Philosophy of Science Part B: Studies in History and Philosophy of Modern Physics, Volume 46, Part B, May 2014, Pages 316-326, DOI: https://doi.org/10.1016/j.shpsb.2013.08.002
[2] Vegt W.; A Continuous Model of Matter based on AEONs, Physics Essays, Volume 8, Number 2, 1995; Equation 119 Page 216, Equation A45 Page 221 and Equation A46 Page 221; DOI: 10.31219/osf.io/ra7ng
[3] Vegt W.; "The Origin of Gravity in "Quantum Light Theory""; OSF Preprints; 14 October 2022; DOI:10.31219/osf.io/n43yd
[4] Vegt W.; The Origin of Gravity; Research & Reviews: Journal of Pure and Applied Physics; Manuscript No. JPAP-22-76022(A); Equation 21 Page 13; Published: 26 October 2022; DOI: 10.4172/2320-24 59.10004 / https://www.rroij.com/open-access/the-origin-of-gravity.php?aid=91966
[5] Joel Kaye, A History of Balance, 1250–1375. The Emergence of a New Model of Equilibrium and its Impact on Thought, April 2014, ISBN: 9781107028456
[6] Kerr, R.P., Schild, A. Republication of: A new class of vacuum solutions of the Einstein field equations. Gen Relativ Gravit 41, 2485–2499 (2009). https://doi.org/10.1007/s10714-009-0857-z
[7] Zachary Dutton, Michael Budde, Christopher Slowe, Lene Vestergaard Hau; ; Observation of Quantum Shock Waves Created with Ultra Compressed Slow Light Pulses in a Bose-Einstein Condensate; Science 28 June 2001; DOI: https://doi.org/10.1126/science.1062527
[8] Vegt W. 2002; The Maxwell-Schrödinger-Dirac Correspondence in Auto Confined Electromagnetic Fields; Equation 3 Page 3; Annales Fondation Louis de Broglie, Volume 27, no 1

[9] Vegt W.; Enhancing precision in electromagnetic force density modulation using LASER control; Journal of Laser Applications; Volume 37, Issue 1, February 2025; DOI: https://doi.org/10.2351/7.0001636
[10] Nowik-Boltyk, P., Dzyapko, O., Demidov, V. et al. Spatially non-uniform ground state and quantized vortices in a two-component Bose-Einstein condensate of magnons. Sci Rep 2, 482 (2012). https://doi.org/10.1038/srep00482
[11] Herrmann Sven, Felix Finke, Martin Lülf, Olga et. al 4 December 2018, Gravitational Redshift Test Using Eccentric Galileo Satellites, Phys. Rev. Lett. **121**, 231102, DOI: 10.1103/PhysRevLett.121.231102
[12] Delva P, Puchades N, Schönemann E, Dilssner F, Courde C et. al 4 December 2018, Gravitational Redshift Test Using Eccentric Galileo Satellites, Phys. Rev. Lett. 121, 231101 – Published; DOI: 10.1103/PhysRevLett.121.231101
[13] Rui Zhang, Sean R. Garner, and Lene Vestergaard Hau;
Creation of Long-Term Coherent Optical Memory via Controlled Nonlinear Interactions in Bose-Einstein Condensates;Phys. Rev. Lett. 103, 233602 – Published 4 December, 2009; DOI: https://doi.org/10.1103/PhysRevLett.103.233602; (https://news.harvard.edu/gazette/story/2001/01/researchers-now-able-to-stop-restart-light/)
[14] Brooks M. and Burkard G.; Electric dipole spin resonance of two-dimensional semiconductor spin qubits; Phys. Rev. B 101, 035204 – Published 30 January, 2020 DOI: https://doi.org/10.1103/PhysRevB.101.035204
[15] Wheeler John Archibald; GEONs, Physical Review Journals Archive, 97, 511, Issue 2, pages 511-526, Published 15 January 1955, Publisher: American Physical Scociety, DOI: 10.1103/PhysRev.97.511:
[16] Baba, T. Slow light in photonic crystals. Nature Photon 2, 465–473 (2008). https://doi.org/10.1038/nphoton.2008.146
[17] Figotin, A., & Vitebskiy, I. (2006). Slow light in photonic crystals. Waves in Random and Complex Media, 16(3), 293–382. https://doi.org/10.1080/17455030600836507
[18] O. Deparis, S. R. Mouchet and B.L.Su; Light harvesting in photonic crystals revisited: why do slow photons at the blue edge enhance absorption; Phys. Chem. Chem. Phys., 2015,17, 30525-30532; https://doi.org/10.1039/C5CP04983K